Research Article

Double-Stranded DNA Damage Assessed with Raman Spectroscopy

Auner AW[1,2] and Thomas JC[1]*

[1]Department of Natural Sciences, University of Michigan-Dearborn, Dearborn, MI 48128, USA
[2]Children's Hospital of Michigan, Detroit Medical Center, Detroit, MI 48201, USA

Abstract

Double stranded DNA breaks [DSBs] and subsequent repair can correct DNA damage or may mistakenly cause mutations leading to cell damage and disease. DSBs can be by measured with Raman spectroscopy, using inelastic scattered light resulting from distinct molecular vibrations from purified DNA samples. With an exposure time of 20 s and 2 accumulations, Raman analysis found circular pBS KS[+] plasmid DNA vibrations were similar to the water blank control. Restriction of the pBS KS[+] single EcoR1 site created linear DNA and significant increases in Raman peaks at 880, 1044, 1084, and 1458 cm^{-1}. To further explore Raman detection of DNA damage, human Jurkat lymphocytes were grown in +/- 16 µg/ml of Bleocin™. DNA from the Bleocin™ treated cells demonstrated enhanced Raman absorption at 880, 1044, 1084, and 1458 cm^{-1} versus untreated cells. Jurkat cells are deficient in the ability to express pro-apoptotic Bax protein and p53, yet Bleocin™ exposure increased TAp73 levels, and subsequently cell death. Due to low interference in biological materials and high sensitivity, Raman spectroscopy is a rapid and simple method to comparatively estimate the extent of relative DSBs. Unlike comet assays, which require analysis of living and dying cells, isolated DNA can be easily recovered from virtually any cell, stored, and DSB analysis done later.

Keywords: Double stranded DNA breaks; Mutation monitoring; p53 independent apoptosis; p73

Introduction

Activation of a host of specific repair mechanisms is dictated by the type(s) of DNA damage [1]. In single stranded DNA repair, the opposite strand is used as a template and repair is highly accurate compared DSB repair, which implements either non-homologous end joining [NHEJ], or homologous recombination [2,3]. Inaccurate repair creates potential DNA mutations, some possibly passing into future generations. As a second unfortunate consequence, DNA damage and repair is linked to cellular aging, and cancer [4,5].

DSBs can arise from elevated numbers of random single stranded breaks or the direct result of UV and x-ray exposure, oxidation, or mutagenic chemical agents. In the absence of a hydroxyl radical, DSBs are thought to result from two or more proximal SSBs [6]. Without a template, DSBs can be repaired in head/head, head/tail, tail/head and tail/tail reconfigurations, and non-homologous chromosomal fusions, all possibly generating inexact base deletions, or insertions during ligation, which increase the likelihood of genomic alteration [3,7]. Cancers, immunodeficiency, and neurodegeneration are some of the health problems associated with dysfunctional NHEJ and DSBs [8]. To repair DSB, homologous recombination [HR] or non-homologous end joining [NHEJ] mechanisms are employed [2]. NHEJ also plays a critical role in normal DNA rearrangements, such as forming different antibodies [9]. The signalling and facilitation of the NHEJ-linked repair process is considered complex and is currently being established.

Raman spectroscopy is a very attractive means to monitor DNA breaks. Resulting from the Raman Effect, Raman spectroscopy measures the inelastic scattered photons. The incoming photon imparts energy to increase the vibrational energy level of the target molecule and then departs with lower energy. The net change in energy is represented as a peak on the Raman spectrum. This peak can be directly related to the identification and structure of that target molecule, in effect it's molecular fingerprint. By itself, water demonstrates a very weak Raman scatter. Conversely, nucleic acids and proteins dissolved in water show a high Raman signal sensitivity in a biological environment. Due to the high sensitivity of modern CCDs and throughput of holographic notch filters, a small sample concentration can still yield a strong Raman signal, taking into account penetration depth from the laser [10]. Raman spectroscopy has been used in biological systems such as determining: sperm viability [11], virus assessment [12], T-Cell activation [13], atherosclerosis [14], breast cancer assessment [15] and cancer diagnostics applied to DNA phosphodioxy moieties in the DNA backbone [10,16].

The objective of this study was to investigate whether double stranded DNA breaks change Raman-detected peaks as a result of changes in the vibrational group frequencies in the DNA backbone. In an earlier study isolated DNA had Raman peaks intensities at 814, 783, 1462, and 1489 cm^{-1} [17]. Raman spectrometry was found capable of differentiating intact circular from restricted plasmid DNA using signature peaks at 1456 and 790 cm^{-1} as observed by Benevides et. al. in a very small 222 bp plasmid [18]. Recently Raman tip scattering combined with Atomic Force microscopy detected DSBs from UVC radiation cleavage at the 3'- and 5'-bonds of deoxyribose [19].

Using Raman microscopy, we observed that standard plasmid pBS KS+ [~3 kb] when restricted at a single site could be differentiated as linear, compared to a circular plasmid. The increase in DSBs and the resultant qualitative increases in vibrational states were easily noted using this high resolution Raman instrument, with significantly low acquisition time and sample concentration detection.

Immortalized human Jurkat lymphocyte cells were employed in this study. They demonstrate effective apoptosis [20,21], albeit with a damaged cell-cycle checkpoint [22]. We examined purified Jurkat cell DNA after exposure to the drug Bleocin™, a member of the

Bleomycin family. Bleomycin is known to target site-specific sugar groups, generating free radicals that induce extensive single and double stranded DNA breaks [23,24]. Bleomycin was also implicated in coordinating the induction of p53 and related family members p73 and p63 to promote apoptosis in lymphocytes and hepatic cells [25]. The enhancement of Raman peaks observed in Bleocin™ treated Jurkat cell DNA vs. controls reinforced the idea that Raman methodology is well suited for qualitative DNA damage assessment [DSBs detection] in purified DNA samples, an effective and complementary methodology to existing DNA damage assays such as the comet assay [26].

Material and Methods

Cell manipulations

The human lymphocyte cell line Jurkat, Clone E61 (ATCC® TIB152), was kindly provided by Dr. Michael Twiner. This pseudo diploid human cell line demonstrated non-attached and suspension-like cell growth. These cells contain several different mutations incapacitating expression of the tumor suppressor p53 and the pro-apoptotic protein Bax [27,28]. Cells were grown in RPMI 1540 medium (InVitrogen, Carlsbad, CA) with 10% (v/v) fetal bovine serum (Atlanta Biologicals, Atlanta, GA) at 37°C in 25 cm² canted neck vent T flasks with membrane inserts (Corning Inc, Corning, NY) in a 37°C, 5% CO_2 atmosphere. Cell passage was between 21 and 29 for the experiments described here. Generally cells were transferred between 4 and 6 days, with an inoculation cell density of approximately 1 X 10⁶/ml. Cell viability was examined using the standard 0.4% Trypan Blue exclusion dye (Sigma Aldrich, St Louis, MO).

Bleocin™ treatment

Bleomycin (Bleocin™) was purchased from Calbiochem EMD Millipore/Merk, (Merck KGaA, Darmstadt, Germany) and dissolved in sterile water. Two days following subculture, Jurkat lymphoma cells were treated with 16 µg/ml of Bleocin™ [29] and DNA later isolated in duplicate 2 days and 4 days after treatment. Bleocin™ treatment of Jurkat cells was previously shown to produce significant numbers of DSBs [21-23].

DNA preparation

Circular plasmid pBS KS⁺ (Stratagene, La Jolla, CA) was isolated from DH5 alpha E. coli using a standard alkaline lysis method with RNase treatment and chloroform deproteinization [30]. DNA was precipitated, and the pellet dissolved in sterile reverse osmosis water. Approximately 2 µg of plasmid DNA was cut with EcoRI 1h, 1U/µg DNA at 37°C. Following removal of protein and re-precipitation, the DNA was re-dissolved in sterile water. Jurkat DNA isolation used a Qiagen total DNA kit (Germantown, MD, USA). Standard RNase and protein removal (chloroform) treatments were included in the isolation [30]. DNA concentration was determined at 260 nm (Nanodrop, Thermco Scientific, Wilmington, DE), and DNA integrity tested using 1.2% w/v agarose gel electrophoresis in TAE buffer, subsequently stained with ethidium bromide [30]. No Tris buffer was used in DNA isolation because it interferes with Raman [17]. Following background (blanking) with water, linear and circular DNA samples dissolved in sterile water were placed on a stainless steel slide for Raman measurement, 145 ng/µl and 100 ng/µl respectively. DNA sample volumes used for Raman measurement volumes were between 15 and 25 µl.

Plasmid DNA state

To assess the relative level of supercoiled, nicked circular, and linear DNA, approximately 250 ng of total pBS KS+ plasmid DNA (uncut) was subjected to 1.2% agarose gel electrophoresis, the gel stained with ethidium bromide, and the bands excised, DNA eluted using a commercial kit (MEGAquick-spin PCR and Agarose Gel DNA Extraction Kit (Bulldog Bio, Portsmouth, NH), and DNA determined using absorbance 260 nm (Nanodrop, Thermco Sci, Wilmington, DE.). Lambda DNA (New England Biolabs, Ipswich, MA) was 48,502 base pairs in length length and was used as a linear DNA standard.

Raman spectroscopic measurements

A Renishaw Raman microscope (RM1000), equipped with a laser wavelength 785 nm was used to record the spectra (Invia Raman Microscope, Renishaw, Gloucestershire, UK). The power of the spectrometer was measured at 2.3 mW. The spectral region of interest was 600-1800 cm⁻¹, where the majority of biological constituents lie. An exposure time of 20 seconds per spectrum was used with an average of two spectral accumulations. DNA was measured in 15 - 25 µl water droplets deposited on a steel slide. Measurements were processed using background subtraction, derivative smoothing, and vector normalization [31]. All experiments were repeated in at least duplicate and figures shown are representative of the data acquired. An average of 4 spectra were taken for each time point and sample for each trial. Spectra were excluded if pre-processing measures failed due to out-of focus measurement or incomplete spectral region of interest. For wavelength and reference peak identification, several key publications were used [32,33].

DNA breakage

In order to verify Bleocin™ - induced DNA double stranded breaks, a TUNEL-like colorimetric assay was used [34]. This assay was linear between 10 ng – 1 µg using linear lambda DNA. Briefly, Bleocin™ treatment for 2 or 4 days was followed by DNA isolation (as described above), including an extensive RNase treatment. Next DNA concentrations were determined using 260 and 280 nm (Nanodrop, Thermco Scientific Wilmington, DE, USA).

To estimate damage, total DNA from 4 separate experiments of untreated and Bleocin™ treated cells was examined in two concentrations (25 – 40 ng). DNA was attached to a well on a 96 well sterile plate by incubation overnight at 10°C in 40 mM Tris-HCl pH 7.4 with 150 mM NaCl. Terminal Transferase was subsequently used to attach dUTP-biotin to free 3' ends of DNA [34]. After streptavidin-conjugated peroxidase (1:200) incubation (Sigma, St. Louis, MO, USA), wells were washed and peroxidase activity was detected after 30 m at 37°C in 0.1% *o*-phenylenediamine dihydrochloride (OPD) (Sigma, St. Louis, MO, USA) in 50 mM phosphate-citrate buffer, pH 5.0, containing 0.03% sodium perborate. Absorbance at 505 nm was measured using a MiniPlate Reader (Bio Rad Labs, Hercules, CA, USA). Terminal Transferase (TdT), Biotin-16-2'-dUTP, and the blocking reagent were from Roche Diagnostics (Mannheim, Germany).

Western blotting

Cells were sub-cultured into 25 mM T-flasks in 10ml of RPMI 1540 with 10% v/v of FCS and penicillin/streptomycin. After growth for two days and the Jurkat cells were treated with 16 µg/ml of Bleocin™ [29] for 0, 2d, or 4d, the cells harvested, washed in 10ml of PBS, and the pellet frozen at –80°C. Cells were sonicated in 2X volumes of 100 mM Tris-HCl, pH 8.0, 100 mM NaCl, 20 mM EDTA, 10 mM DTT, 100µM phenylmethylsulfonyl fluoride (PMSF) and 50µg/ml leupeptin. For each lane, 50µg of soluble total protein extract was separated on a 10% or 12% (w/v) SDS-Laemmli gel, blotted to nitrocellulose, and stained

with antibodies anti-53BP1 (Bethyl Laboratories, Montgomery, TX), p73 (N1C1) (GeneTex, Irvine, CA), or anti-tubulin (Developmental Studies Hybridoma Bank, Univ. of Iowa, IA). Secondary antibodies were coupled to peroxidase to facilitate enzymatic detection of proteins.

Results

Raman peaks corresponding to sugar-phosphate backbone vibrations and DNA base vibrations were detected in linear pBS KS+, and not in circular plasmid. These Raman peaks were coincident with DNA double stranded breaks (DSB) caused by the single EcoR1 DNA restriction digest (Figure 1). Enhanced intensities at 880, 1044, 1084, and 1456 (as well as the 1456/1485 ratio) were observed after a single EcoR1 digest, further increasing in a double digest (EcoR1 and Xmn 1) (Figure 1). The observed DNA peaks captured by Raman are likely generated by inter and intra-molecular vibrations in the DNA, and they correspond to specific DNA constituents as described in Table 1, adapted from [32].

When pBS KS+ uncut plasmid was subjected to electrophoresis, most of the DNA preparation migrated in a supercoiled circular form (95%). The remainder of DNA (both liner and nicked circular) was approximately 5% of the total sample, as determined by absorption at 260 nm following DNA recovery from agarose gel electrophoresis.

In a comparison experiment, human Jurkat genomic DNA digested with EcoRI, or melted to convert DNA to single-stranded molecules resulted in enhanced Raman peak intensities compared to untreated Jurkat DNA (Figure 2). When EcoR1 digestion of Jurkat genomic DNA
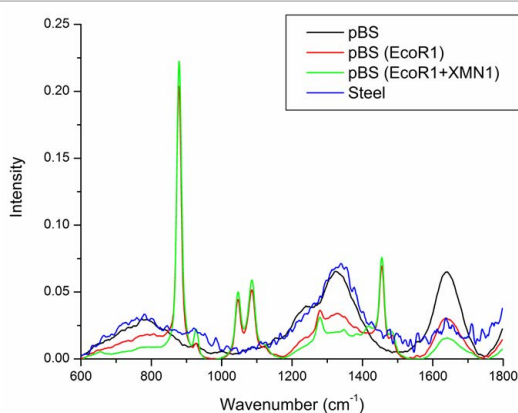

Figure 1: Raman spectra for plasmid pBS KS+, single and double digests and double strand breakage. There are single EcoR1 and Xmn1 restriction sites in the pBS KS+ plasmid. Enhanced intensities of restricted DNA were seen at 880, 1044, 1084, 1456, cm⁻¹ (and the 1485/1456 ratio, not shown). We include the raw water/steel measurements, subsequently subtracted from each sample Raman scan.

Wave number (cm⁻¹)	Macromolecule	Vibration Source
764-772	Cytosine, Thymine	Pyrimidine ring breathing
880	DNA	Possible C-C backbone vibration
926	DNA	Possible C-C backbone vibration
1044	DNA	PO_4^{-3} stretch backbone
1084	DNA	PO_2 stretch backbone
1280	DNA	Nucleic Acid Vibration
1456	DNA	Deoxyribose or Guanine vibrations
1485	Adenine, Guanine	Purine ring breathing
1645	DNA or substrate	DNA ring breathing or strong substrate artifact

Table 1: Peaks assignments for Raman spectra of DNA. (For references see [29,30]).
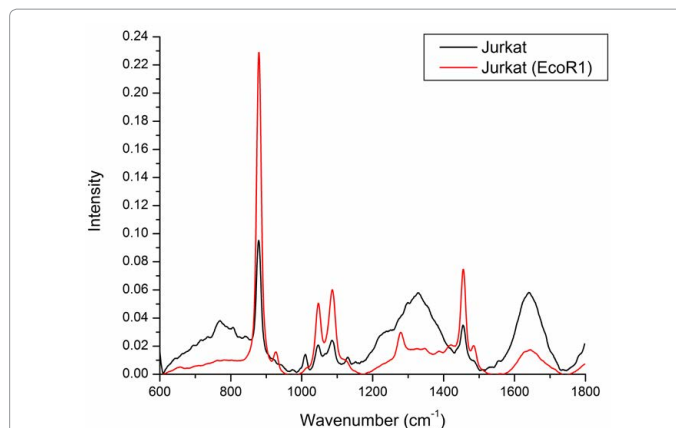
Figure 2: Raman spectra of human Jurkat native DNA (black), EcoR1 digested (red). Note the enhanced intensities following EcoR1 restriction at 880, 1044, 1084, and 1456 cm⁻¹.
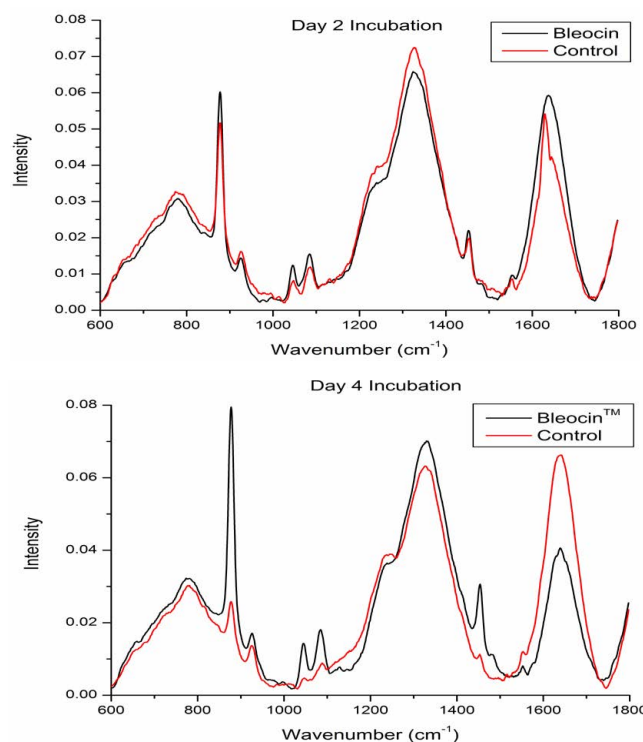
Figure 3: Three Raman spectra of control and Bleocin™ treated cell DNA after 2 (A) and 4 (B) day. Cell viability: controls were C day 2 (90%), C day 4 (93%), Bleocin™ day 2 (54%), Bleocin™ day 4 (16%). Generally, cells divided after 24h in controls, whereas cell division, based on cell counts, was impaired in Bleocin™ treated samples (not shown). Enhanced 880, 1044, 1084, and 1456 cm⁻¹ peaks are again noted in 2 and 4d Bleocin™ treated cells.

was completed, increases in Raman peaks of 880, 1044, 1084, and 1456 cm⁻¹ compared to uncut Jurkat DNA were also recorded (Figure 2).

Bleocin™ is a compound known to create DSBs in DNA [23,24]. Cell viability in the untreated cells was substantial: 90% and 93% of the cells viable at day 2 and 4 respectively. Treatment with 16 μg/ml Bleocin™ resulted in reduced cell viability: 54% and 16% at day 2 and 4 respectively, providing cell swelling and blebbing characteristic of apoptosis [35,36]. Likewise, isolated DNA of control and Bleocin™ treated cells were subjected to Raman analysis (Figures 3A and 3B).

Although the Raman peak heights of 880, 1044, 1084, and 1456 cm^{-1} increased with Bleocin™ treatment, the increases were less pronounced that those observed following Jurkat DNA restriction digest (Figure 2). In cells untreated or treated with Bleocin™, the apparent molecular masses of isolated DNA were largely greater than 24 kB, with signs of DNA cleavage (some smearing) from the Bleocin™-treated groups (Figure 4).

To confirm enhanced DNA breakage in Bleocin™ treated cells compared to controls, a 3' end labeling biotin - dUTP procedure was used [34-36]. Two day Bleocin™ treated cells contained DNA with 1.12 (0.05 SD) (or 12% free ends) in excess of controls. When treatment was extended to 4d Bleocin™, 1.20 (0.05 SD) (or 20% free ends above controls) were estimated. This data represents 4 separate DNA treatments and isolations.

Western blot analysis indicated the 2 and 4 day incubations with
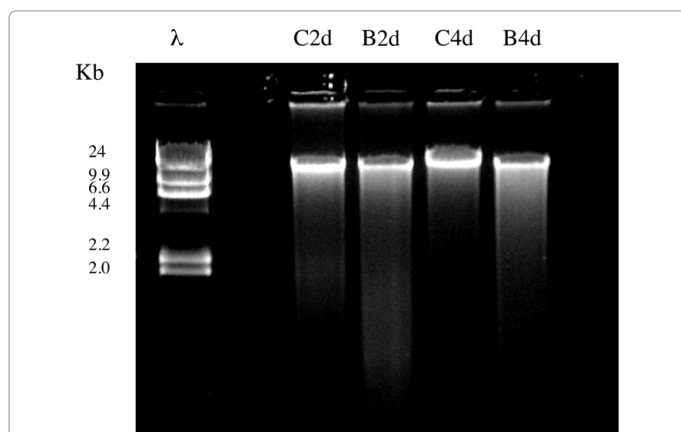
Figure 4: Approximately 1 μg/lane of genomic DNA isolated from Jurkat cells after 2 and 4 days of Bleocin™ treatment. Kilobase markers are indicated with the Hind III ladder. Genomic DNA is largely intact and greater than 24 KB. Lambda Hind III marker was used as a size reference. Slightly more smearing in DNA from cells in the Bleocin™ treatments was observed.
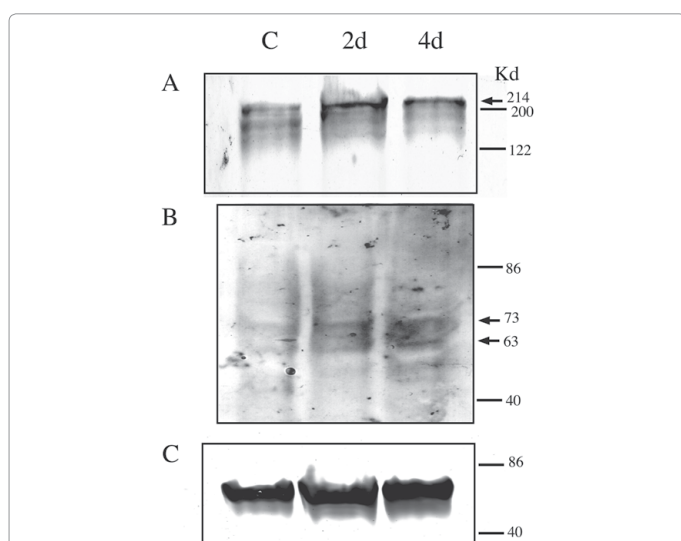
Figure 5: G50μg of total protein extract/lane from C(ontrol) or cells treated with16 μg/ml Bleocin™ for 2 days or 4 days. Samples were separated on a 10% (A, C) or 12% (B) (w/v) SDS-Laemmli gel, blotted to nitrocellulose. Blots were reacted with (A) anti - 53BP1 (214 Kd), (B) anti - TAp73 (73Kd), or (C) anti – alpha tubulin (50 Kd) antibodies. Data shown is a representative blot from three experiments.

Bleocin™ promoted the accumulation of 53BP1 compared to control cells (Figure 5A). 53BP1 is a critical repair protein that binds chromatin near double strand breaks and promotes nonhomologous end-joining to repair double strand breaks [37]. An isoform of p53, TAp73 protein is known to facilitate apoptosis in Jurkat cells and hepatocytes following DNA damage [35,38,39]. Here, p73 and p63 kD proteins were accumulated above controls at 2d and 4d of Bleocin™ treatment (Figure 5B) [25,40]. For a loading control, blots were also reacted with an anti – α tubulin antibody, subsequently revealed with a secondary antibody linked to alkaline phosphatase (Figure 5C).

Discussion and Conclusion

Following DNA cleavage with restriction enzymes, enhanced Raman peaks were detected at 880, 1044, 1084, and 1456 cm^{-1} in both plasmid and human genomic DNA (Figures 1 and 2). One report considered the DNA specific Raman peaks only at 1080 cm^{-1}, and 1232 cm^{-1} [41], with the 1468 cm^{-1} ascribed to protein. Because all DNA samples were deproteinized pre- and post- DNA restriction, the 1468 peak observe here may more likely correspond to Deoxyribose or Guanine vibrations and/or purine ring breathing as previously reported [32,33]. The observed increased scattering in pBS KS+ for single and double restriction digests compared to uncut circular plasmid reflected greater backbone flexibility and stretch, as the plasmid was no longer confined to a circular configuration (Table 1). One peak at 1645 cm^{-1}, seen in restriction-digested samples, may be a substrate artifact or a complex interaction between double-stranded helical interaction of nitrogenous bases and the backbone (Table 1; Figures 1 and 2). These peak identities have a distinct similarity to those observed in previous study of DNA breakage [17,33].

The major difference in this analysis and earlier studies is the increased sensitivity for DNA breakage with our instrument. Importantly, this study noted negligible scattering for circular plasmid vibrations perhaps due to the small DNA concentrations tested, the fast data acquisitions of the Invia Raman Microscope, the lack of any Tris buffer contamination throughout the protocol [17], and potential differences in DNA state following plasmid isolation (i.e. DNA sheering during the isolation). Here, as noted, plasmid DNA (uncut) was predominantly circular (95%) following recovery from *E. coli*. Raman measurements here provided the means to differentiate intact and restricted plasmid DNA (e.g. enhanced DSBs).

EcoR1 digestion of Jurkat DNA resulted in significant peaks at 880, 1044, 1084, and 1456 cm^{-1} versus uncut DNA samples and denatured (ss) DNA (Figure 2). The extent of DNA digestion/breakage-enhanced peaks were generally more pronounced than those observed in the pBS KS+ experiments, perhaps due to the multiple EcoR1 restriction sites in the human genome (vs. one in pBS KS+) creating numerous and varied length DNA fragments that increased in vibrational frequencies. We speculate that if pBS KS+ DNA was repeatedly digested by a series of restriction enzymes, the increased fragment numbers and smaller DNA lengths, may elevate light scattering and increase the peaks at 880, 1044, 1084 and 1456 cm^{-1} above a single digest. In other words, moving from a circular to a linear structure may represent a large relative change in the Raman signals acquire from a DNA sample, while further digestion of that linear molecule to smaller linear molecules may gradually increase spectral peak augmentation.

Comparative Raman signals qualitatively reflect DSBs; however a linear relationship of peak height to number of DSBs may not be realized. Additional factors such as dissimilar fragment lengths and fragment to fragment interactions between carbonyl and backbone

phosphodiester groups or DNA and the levels of divalent cations may complicate simple quantitative estimates of DSBs [42]. Using an end labeling method [34], Bleocin™ treatment did lead to higher 3' end labeling compared to untreated controls. While the relative differences between control and treated cells were maintained, the degree of peroxidase-derived product was quite variable from experiment to experiment. For this reason, a correlation analysis between the Raman method and the end filling method was not possible.

The p53 - deficient Jurkat cell line contains mutations in the DNA-binding domain of the p53 gene [27]. In addition, several single base deletions and additions in the polyguanine region within the open reading frame of the BAX gene also resulting in no production of the pro-apoptotic BAX protein [28]. In spite of these mutations, Jurkat cells undergo p53-independent apoptosis, likely relying on p73, and take advantage of p38 and/or JNK MAP activation [43]. The promoter upstream of the TA-p73 gene contains several E2F binding sites [39,40]. E2F binding to p73 promoter regions likely plays a significant role in the p53-independent activation and induced cell death of hepatic carcinoma cells [25] and T cells [39,40,44]. However the regulation of p73 and p63 in lymphocytes may also provide anti-apoptotic signals, reflecting the complexity of p53/p73/p63 interactions within different cell types and as a result of different cell stresses [45].

Bleomycin, is known to arrest the cell cycle at G2 phase [22] and subsequent DNA damage and repair would then take place in these Jurkat cells [46]. Given defective G1 checkpoint regulation, DNA repair of DSB by Jurkat cells is considered rather robust, where radiation and filter elution at pH 9.6 demonstrated DSB - repair to be greater than 50% of all radiation-induced DSBs incurred [47].

Damage to Jurkat lymphoma cellular DNA results from treatment with the chemotherapy drug Bleocin™, a compound known to induce both SSBs and DSBs [21,23,24]. In studies presented here, Bleocin™ treatment caused general cell viability to decline in (Figure 3), and the genomic DNA appeared slightly smaller in molecular mass compared to controls (Figure 4) after incubation for 2 and 4 days. Raman peaks at 880, 1044, 1084, and 1456 cm^{-1} were notably greater in the Bleocin™ -treated versus untreated controls (Figure 3). These results support the idea that, like EcoR1 digestion (Figures 1 and 2), an increase in the number of DSBs resulted from exogenous Bleocin™ treatment.

Differing from an exclusive DSB agents such as cytolethal distending toxin [48], Bleocin™ - mediated cell toxicity was chiefly attributed to DSBs in DNA [35]. Importantly, high dose Bleocin™ treatment caused DSBs that were 300 times more toxic to Chinese hamster fibroblasts (CHO) cells compared to SSBs [49]. Low doses of bleomycin induce SSBs, themselves capable of inducing apoptosis only when given extensive incubation times [35]. Here the use of high doses of Bleocin™ and simultaneous enhanced cellular toxicity suggest that high levels of DSBs in these treated cells was responsible for rapid apoptosis and cell death [35]. Comet assays can employ neutral and alkaline analysis, and using specific software may provide more contrast between SSB and DSB [50]. In pilot experiments, temperature denaturation of linerized pBS KS+ plasmid DNA (EcoR1 digested) or Jurkat DNA demonstrated a slight increase in Raman DNA peaks compared non-denatured linerized plasmid DNA. Finally, DSBs can also be caused by free radicals or proximal (and under-estimated) SSBs along the same DNA strand [6,51].

In comparison, DNA base analogues such as BrdU (bromodeoxyuridine) are less toxic than Bleocin™, incorporate in place of thymidine, and temporarily repress DNA replication until repair is completed [52-54]. Excision-repair coupled to transcription further minimizes mutations resulting from DNA base analogue substitution [55]. Because SSBs are also efficiently repaired by excision and repair (compared to DSBs) [56], and due to the marked decline in Jurkat cell viability in Bleocin™ experiments (Figure 3), Raman spectroscopy may reflect largely DSB signature spectra in DNA prepared from Bleocin™ treated cells.

The ease of determining DNA breakage status from isolated DNA using Raman spectroscopy may facilitate the study of homologous recombination (HR) or non-homologous end joining (NHEJ) [2]. Southern blots can be used as a general measure of DNA damage; however the procedure is not easily amended to an applied diagnostic [57]. The popular Comet assay (neutral for DSB and alkaline for all DNA breaks) is an effective method for the discrimination of DSB and SSB DNA breaks, however cell extraction, cell-electrophoresis, and relative apoptotic comet tail measurements provide SSB and DSB data of only the surviving cells [26,58]. Other PCR-based DNA damage assays or enzyme-based methods can be very accurate, but are tedious, gene or gene family specific, and are not easily applicable to DSB and endogenous DNA assessment *in vivo* [3,7,59]. Detecting DSBs from previously purified DNA with Raman spectroscopy is advantageous as the approach is rapid, and it does not require special care of cells and image/pixel counting software, as does the common comet assay. Furthermore, isolated and purified DNA can be stored and relative DNA breakage determined at a later date.

Acknowledgement

References

1. Lindahl T, Wood RD (1999) Quality control by DNA repair. Science 286: 1897–1905.

2. Symington LS, Gautier J (2011) Double-strand break end resection and repair pathway choice. Annu. Rev. Genet 45: 247–271.

3. Anson RM, Mason PA, Bohr VA (2006) Gene-specific and mitochondrial repair of oxidative DNA damage. Methods Mol. Biol 314: 155–181.

4. Hasty P, Campisi J, Hoeijmakers J, van Steeg H, Vijg J (2003) Aging and genome maintenance: lessons from the mouse. Science 299: 1355–1359.

5. Woditschka S, Evans L, Duchnowska R, Reed TL, Palmieri D, et al. (2014) DNA double-strand break repair genes and oxidative damage in brain metastasis of breast cancer. J Natl Cancer Inst 106: 1-13.

6. Krisch RE, Flick MB, Trumbore CN (1991) Radiation chemical mechanisms of single- and double-strand break formation in irradiated SV40 DNA. Radiation Res 126: 251-259.

7. Lloyd AH, Wang D, Timmis JN (2012) Single molecule PCR reveals similar patterns of non-homologous DSB repair in tobacco and Arabidopsis. PloS ONE 7: 1-10.

8. Burma S, Chen BP, Chen DJ (2006) Role of nonhomologous end joining (NHEJ) in maintaining genomic integrity. DNA Repair 5: 1042–1048.

9. Lieber MR, Ma Y, Pannicke U, Schwarz K (2004) The mechanism of vertebrate nonhomologous DNA end joining and its role in V(D)J recombination. DNA Repair 3: 817–826.

10. Stone N, Kendall CA (2005) Raman spectroscopy for early cancer detection, diagnosis and elucidation of disease-specific biochemical changes. In: Emerging Raman applications and techniques in biomedical and pharmaceutical fields. Matousek P and Morris MD (eds), 315–346, Springer Berlin, Heidelberg, Germany.

11. Sanchez V, Redmann K, Wistuba J, Wübbeling F, Burger M, et al. (2012)

Oxidative DNA damage in human sperm can be detected by Raman microspectroscopy. Fertility and Sterility 98: 1124-1129.

12. Hamden KE, Bryan BA, Ford PW, Xie C, Li YQ, et al. (2005) Spectroscopic analysis of Kaposi's sarcoma-associated herpes virus infected cells by Raman tweezers. J Virol Methods 129: 145-151.

13. Mannie MD, McConnell TJ, Xie C, Li YQ (2005) Activation-dependent phases of T cells distinguished by use of optical tweezers and near infrared Raman spectroscopy. J Immunol Methods 297: 53-60.

14. Nogueira GV, Silveira L, Martin AA, Zangaro RA, Pacheco MT, et al. (2005) Raman spectroscopy study of atherosclerosis in human carotid artery. J Biomed Opt 10: 031117.

15. Haka AS, Shafer-Peltier KE, Fitzmaurice M, Crowe J, Dasari RR, et al. (2005) Diagnosing breast cancer by using Raman spectroscopy. Proc Natl Acad Sci USA 102: 12371-12376.

16. Auner A, Kast R, Rabah R, Poulik J, Klein M (2013) Conclusions and data analysis: 6-year Study of Raman Spectroscopy of solid tumors at a major pediatric institute. Pediatr Surg Int 29: 129-140.

17. Serban D, Benevides JM, Thomas GJ Jr (2002) DNA secondary structure and raman markers of supercoiling in Escherichia coli plasmid pUC19. Biochemistry 41: 847-853.

18. Benevides JM, Serban D, Thomas GJ (2006) Structural perturbations induced in linear and circular DNA by the architectural protein HU from *Bacillus stearothermophilus*. Biochemistry 45: 5359–5366.

19. Lipiec E, Sekine R, Bielecki J, Kwiatek WM, Wood BR (2014) Molecular characterization of DNA double strand breaks with tip-enhanced Raman scattering. Angew Chem Int Ed Engl 53: 169-172.

20. Schneider U, Schwenk U, Bornkamm G (1977) Characterization of EBV-genome negative "null" and "T" cell lines derived from children with acute lymphoblastic leukemia and leukemic transformed Non-Hodgkin lymphoma. Int J Cancer 19: 621-626.

21. Weiss A, Wiskocil RL, Stobo JD (1984) The role of T3 surface molecules in the activation of human T cells: a two-stimulus requirement for IL-2 production reflects events occurring at a pre-translational level. J. Immunology 133: 123-128.

22. Arai M, Sato H, Kobayashi H, Suganuma M, Kawabe T, et al. (2004) Selective inhibition of bleomycin-induced G2 cell cycle checkpoint by simaomicin alpha. Biochem Biophys Res Commun 317: 817-822.

23. Povirk L (1996) DNA damage and mutagenesis by radiomimetic DNA-cleaving agents: Bleomycin, Neocarzinostatin and other Enediynes. Mutation Research/Fundamental and Molecular Mechanisms of Mutagenesis 355: 71-89.

24. Povirk LF, Han YH, Steighner RJ (1989) Structure of bleomycin-induced DNA double-strand breaks: predominance of blunt ends and single-base 5' extensions. Biochemistry 28: 5808–5814.

25. Seits SJ, Schleithoff ES, Koch A, Schuster A, Teufe A, et al. (2010) Chemotherapy-induced apoptosis in hepatocellular carcinoma involves the p53 family and is mediated via the extrinsic and intrinsic pathway. Int J Cancer 126: 2049-2066.

26. Olive PL, Banath JP (2006) The comet assay: a method to measure DNA damage in individual cells. Nat. Protocols 1: 23–29.

27. Cheng J, Haas M (1990) Frequent mutations in the p53 tumor suppressor gene in human leukemia T-cell lines. Mol Cell Biol 10: 5502-5509.

28. Brimmell M, Mendiola R, Mangion J, Packham G (1998) BAX frameshift mutations in cell lines derived from human haemopoietic malignancies are associated with resistance to apoptosis and microsatellite instability. Oncogene 16: 1803-1812.

29. CALBIOCHEM (2002) BLEOCIN™ A potent antibiotic for the selection of Bleomycin resistance. Information Brochure.

30. Maniatis T, Fritsch EF, Sambrook J (1982) Molecular cloning: A laboratory manual. Cold Spring Harbor Laboratory, Cold Spring Harbor, Cold Spring Harbor, NY.

31. Cao A, Pandya AK, Serhatkulu GK, Weber RE, Dai H, et al. (2007) A robust method for automated background subtraction of tissue fluorescence. J Raman Spectroscopy 38: 1199–1205.

32. Movasaghi Z, Rehman S, Rehman IU (2007) Raman spectroscopy of biological tissues. Appl Spectroscopy Rev 42: 493-541.

33. Benevides JM, Thomas GJ (1983) Characterization of DNA structures by Raman spectroscopy: High-salt and low-salt forms of double helical Poly(dG-dQ in H21 and D20 solutions and application to B, Z and A-DNA. Nucleic Acids Research 11: 5747-5761.

34. Kurasaki M, Sun Y, Komori M, Miyajima M, Hosokawa T, et al. (2012) Measurement of DNA damage by terminal deoxynucleotidyl transferase reaction. Advances in Biological Chemistry 2: 243-247.

35. Tounekti O, Pron G, Belehradek J, Mir LM (1993) Bleomycin, an apoptosis-mimetic drug that induces two types of cell death depending on the number of molecules internalized. Cancer Res 53: 5462-5469.

36. Vemole P, Tedeschi B, Caporossi D, Maccarrone M, Melino G, et al. (1998) Induction of apoptosis by bleomycin in resting and cycling human lymphocytes. Mutagenesis 13: 209-215.

37. Panier S, Boulton SJ (2014) Double-strand break repair: 53BP1 comes into focus. Nature Rev. Mol. Cell Biol 15: 7-18.

38. Karpinich NO, Tafani M, Schneider T, Russo MA, Farber JL (2006) The course of etoposide-induced apoptosis in Jurkat cells lacking p53 and Bax. J of Cellular Physiology 208: 55-63.

39. Tophkhane C, Yang SH, Yunbo Jiang Y, Ma Z, Subramaniam D, et al. (2012). p53 inactivation upregulates p73 expression through E2F-1 mediated transcription. PLoS One 7, e43564.

40. McKeon FD (2004) p63 and p73 in tumor suppression and promotion. Cancer Research and Treatment 36: 6-12.

41. Patel II, Trevisan J, Singh PB, Nicholson CM, Krishnan RK, et al. (2012) DNA alterations exclusively located in epithelial cells segregate prostate tissues on the basis of risk to adenocarcinoma. Mutagenesis 27: 132–133.

42. Duguid J, Bloomfield VA, Benevides J, Thomas GJ (1993) Raman spectroscopy of DNA-metal complexes. I. Interactions and conformational effects of the divalent cations: Mg, Ca, Sr, Ba, Mn, Co, Ni, Cu, Pd, and Cd. Biophys J 65: 1916-1928.

43. Aresvik DM, Pettersen RD, Abrahamsen TG, Wright MS (2010) 5-Fluorouracil-induced death of Jurkat T-Cells – A role for caspases and MCL-1. Anticancer Research 30: 3879-3888.

44. Freebern WJ, Smith JL, Chaudhry SS, Haggerty CM, Gardner K (2003) Novel cell-specific and dominant negative anti-apoptotic roles of p73 in transformed leukemia cells. J. Biol. Chem 278: 2249-2255.

45. Tebbi A, Guittet O, Cottet MH, Vesin MF, Lepoivre M (2011) TAp73 induction by nitric oxide: Regulation by checkpoint kinase 1 (CHK1) and protection against apoptosis. J. Biol. Chem 286: 7873-7884.

46. Scarsbrook AF, Thakker RV, Wass JHS, Gleeson FG, Phillips RR (2008) Multiple endocrine neoplasia: Spectrum of radiologic appearances and discussion of a multi-technique imaging approach. RadioGraphics 26: 433-451.

47. Evans HH, Ricanati M, Horng MF, Jiang Q, Mencl J, et al. (1993) DNA double-strand break rejoining deficiency in TK6 and other human B-lymphoblast cell lines. Radiation Res 134: 307-315.

48. Shenker BJ, Dlakic M, Walker LP, Besack D, Jaffe E, et al. (2007) A novel mode of action for a microbial-derived immunotoxin: The cytolethal distending toxin subunit B exhibits phosphatidylinositol 3,4,5-triphosphate phosphatase activity. The Journal of Immunology 178: 5099–5108.

49. Tounekti O, Kenani A, Foray N, Orlowski S, Mir LM (2001) The ratio of single-to double-strand DNA breaks and their absolute values determine cell death pathway. British Journal of Cancer 84: 1272–1279.

50. Angelis K, Dusinska M, Collins A (1999) Single cell gel electrophoresis; detection of DNA damage at different levels of sensitivity. Electrophoresis 20: 2133–2138.

51. Balagurumoorthy P, Adelstein SJ, Kassis AI (2011) Novel method for quantifying radiation-induced single-strand-break yields in plasmid DNA highlights tenfold discrepancy. Anal Biochem 417: 242–246.

52. Thomas JC, Katterman FRH (1992) 5-Bromodeoxyuridine inhibition of cytokinin induced radish cotyledon expansion. Plant Science 83: 143-148.

53. Thomas JC, Nessler C, Katterman FRH (1989) Interruption of somatic embryogenesis in *Daucus carota* L. by 5-bromodeoxyuridine. Plant Physiology 90: 921-927.

54. Hancock A, Priester C, Kidder E, Keith JR (2009) Does 5-bromo-2, deoxyuridine (BrdU) disrupt cell proliferation and neuronal maturation in the adult rat hippocampus in vivo. Behavioral Brain Research 199: 218-221.

55. Kim N, Jinks-Robertson S (2010) Abasic sites in the transcribed strand of yeast DNA are removed by transcription-coupled nucleotide excision repair. Mol Cell Biol 30: 3206–3215.

56. Sanders MF, Bowman JL (2012) Genetic analysis: An integrated approach, Pearson.

57. Evert BA, Salmon TB, Song B, Jingjing L, Siede W, et al. (2004) Spontaneous DNA damage in *Saccharomyces cerevisiae* elicits phenotypic properties similar to cancer cells. J. Biol. Chem 279: 22585–22594.

58. Kozak J, West CE, White C, Da Costa-Nunes JA, Angelis KJ (2009) Rapid repair of DNA double strand breaks in *Arabidopsis thaliana* is dependent on proteins involved in chromosome structure maintenance. DNA Repair 8: 413–419.

59. ESCODD and European Standards Committee on Oxidative DNA Damage (2003) Measurement of DNA oxidation in human cells by chromatographic and enzymatic methods. Free Radic Biol Med 34: 1089-1099.